BENCHMARK SOLUTION FOR THE CATEGORY 3—PROBLEM 2: CASCADE–GUST INTERACTION

Edmane Envia
National Aeronautics and Space Administration
Glenn Research Center
Cleveland, Ohio 44135

ABSTRACT

The benchmark solution for the cascade-gust interaction problem is computed using a linearized Euler code called LINFLUX. The inherently three-dimensional code is run in the thin-annulus limit to compute the two-dimensional cascade response. The calculations are carried out in the frequency-domain and the unsteady response at each of the gust's three frequency component is computed. The results are presented on modal basis for pressure perturbations (i.e., acoustic modes) as well as velocity perturbations (i.e., convected gust modes) at each frequency.

INTRODUCTION

The periodic impingement of the wakes of a rotor on a downstream stator is one of the principal sources of turbomachinery noise and a significant contributor to the overall noise produced by modern aircraft engines. As such, this source has been the focus of many analytical modeling efforts over the years, but with the recent emergence of computational aeroacoustics (CAA) as a viable alternative, the emphasis has now shifted away from analytical approaches to purely numerical ones. Naturally, as in the other aeroacoustic problems of engineering interest, the success of CAA is predicated on the availability of efficient computational algorithms and robust boundary conditions. In theory, a candidate algorithm must be able to handle the generation and propagation of sound waves in the presence of complex geometries, and through non-uniform media, with no dispersion or dissipation; the boundary conditions must be able to handle the passage of the unsteady disturbances through the boundaries of the computational domain with no reflection; and both of these requirements must be satisfied at frequencies of engineering interest. The usefulness of CAA is, therefore, greatly dependent on the extent to which all of these conditions are met, and its practicality is dependent on the resource requirements (hardware and CPU time) that must be expended to achieve reasonably accurate solutions for design and analysis purposes. The proposed two-dimensional benchmark problem was designed to address principally the question of usefulness. The issue of practicality is best addressed using a three-dimensional benchmark problem, which is postponed until the next workshop.

BENCHMARK SOLUTION

The solution for the benchmark problem was obtained using a code called LINFLUX which is based on a linearized frequency-domain method for solving the three-dimensional inviscid unsteady flow equations. The method has been extensively documented and validated using two- and three-dimensional test cases (see refs.1 through 4) and so will not be covered here. LINFLUX is actually part of a collection of codes which also includes a grid generation package called TIGER, a steady nonlinear inviscid flow solver called TURBO, and a set of processing routines for generating the harmonic content of the incident disturbance (i.e., acoustic, vortical and entropic). The information obtained from all three codes is used to run LINFLUX, which calculates the acoustic response produced by the incident disturbances on the blade row at specified harmonics of the rotor-stator blade passing frequency.

Computational grid

Since LINFLUX cannot be easily modified to run in two-dimensional mode, the cascade geometry was "wrapped" around an annulus with a mean radius of $\bar{R} \approx 5.7c$ and a hub-to-tip radius ratio of 0.996 (see Figure 1a). The result is a blade row that is, strictly speaking, three-dimensional, but owing to its extremely small spanwise extent (only ~2.3% of the vane chord) would result in solutions that are effectively two-dimensional in nature

depending only on the axial and tangential coordinates (see Figure 1b). Since the solution is computed in the frequency-domain, only one passage of the blade row is needed when appropriate periodicity conditions are enforced (see Figure 1c). To ensure sufficient resolution of the mean flow details and the response to the highest frequency gust (i.e., reduced frequency of $9\pi/4$), a grid with 301×81×7 points in the axial, tangential and radial directions was created. The grid is packed near the airfoil boundaries and also in the vicinity of the leading edge (see Figure 1d).

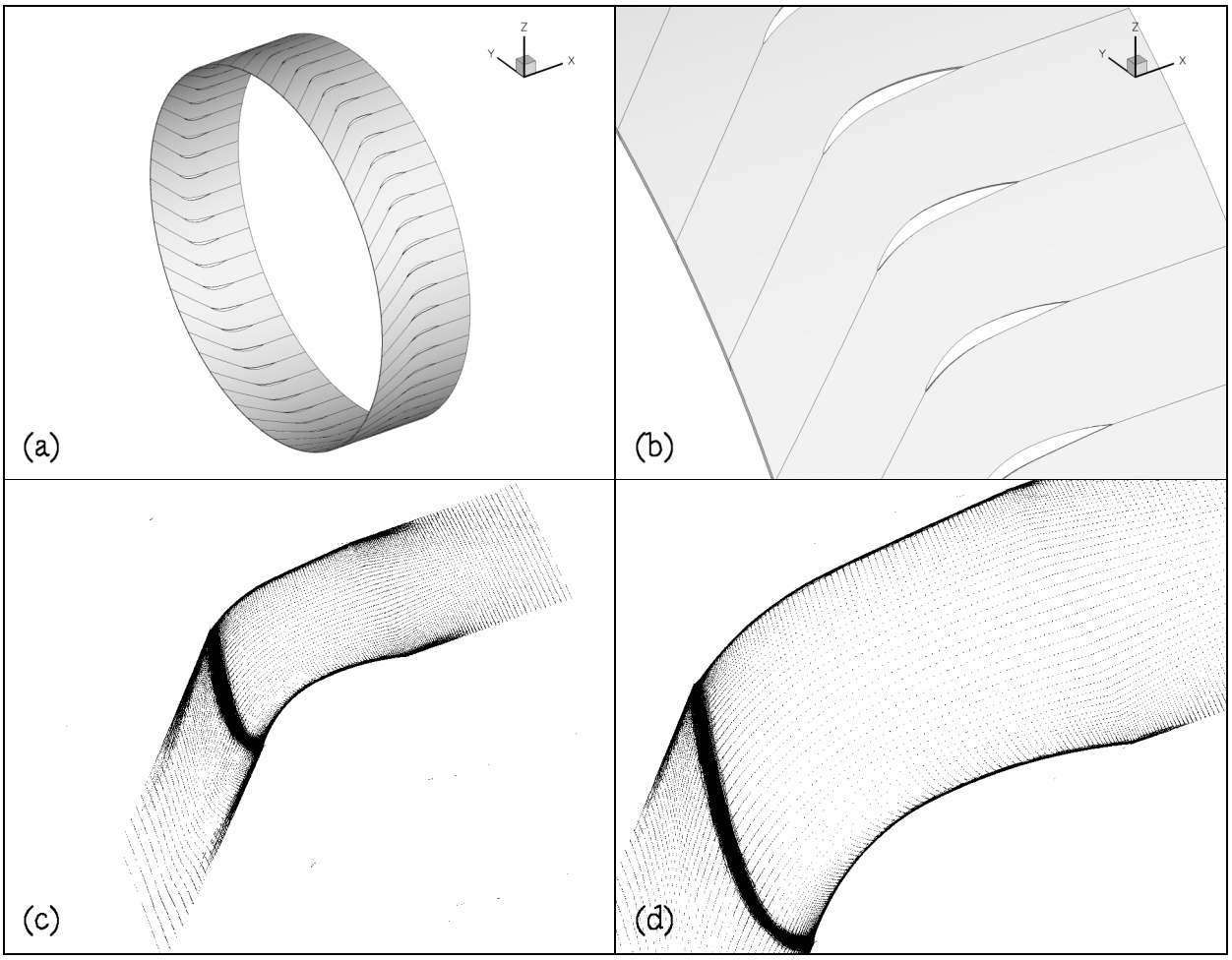

Figure 1. Three-dimensional thin annulus representation of the two-dimensional geometry of the benchmark problem (a). Hub-to-tip radius ratio is 0.996 (b) resulting in a solution that is effectively independent of the radial coordinate. The passage grid, which has 301×81×7 points in the axial, tangential and radial directions, is shown for the radial grid index = 4 (c). The grid is packed near the airfoil surfaces and in the vicinity of the leading edge (d).

Steady flow solution

The steady flow needed as input to LINFLUX was computed using the nonlinear Euler code called TURBO (see ref. 5) on the grid discussed in the previous section. The computation was run to convergence as indicated on the left side of Figure 2. The graph shows the convergence history of the error (residual) as a function of the iteration count. The residual was reduced by five orders of magnitude after 25,000 iterations, but the iteration process was continued a further 10,000 steps to ensure convergence of all relevant flow parameters. On the right, the resulting Mach number distribution after 35,000 iterations is shown.

For the purposes of the presentation, the $x-\theta$ plane corresponding to the radial grid index = 4 is unrolled and both the geometry and solution are duplicated. In this two-dimensional representation, *x* denotes the horizontal

coordinate, and $y = r\theta$ denotes the vertical coordinate. Clearly the steady flow is uniform along the *y*-direction at the inflow and outflow planes ($x = \mp 1.5c$) except for the presence of a thin wake downstream of the vane trailing edge produced as a result of numerical dissipation. The flow over the vane itself behaves as expected with steady loading evident in the form of low Mach number values (corresponding to high pressure values) on the pressure side and high Mach number values (corresponding to low pressure values) on the suction side of the vane.

Representative averaged flow quantities at the inflow and outflow planes obtained using TURBO are shown in Table 1. It should be noted that the inflow plane flow angle is an input in TURBO. Using the isentropic flow relations, the stagnation pressure and temperature at the inflow and outflow planes can be readily computed and found to be equal to 1.00000 satisfying the other requirements specified in the benchmark problem.

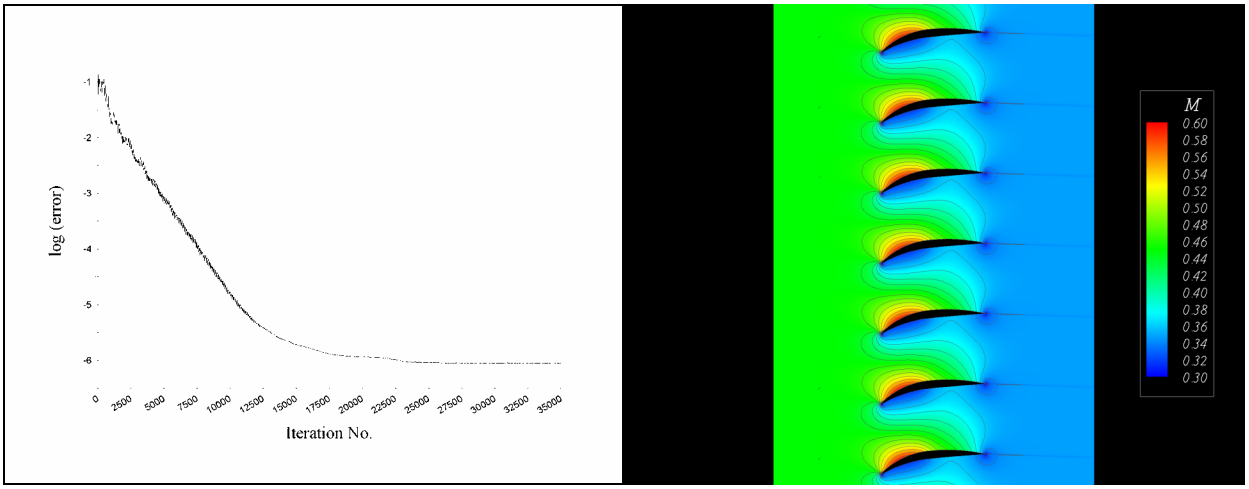

Figure 2. Steady flow obtained using the TURBO code. Convergence history over 35,000 iterations is shown on the left and the resulting Mach number distribution is shown on the right. There is evidence of slight numerical dissipation in the form of a thin wake downstream of the vane trailing edge.

	Mach No.	Static Pressure	Static Temperature	Flow Angle (deg.)
Inflow Plane	0.44958	0.87049	0.96115	36.00*
Outflow Plane	0.34704	0.92000	0.97648	1.71

Table 1. Steady flow quantities at the inflow and outflow planes of the computational domain after 35,000 iterations. The flow variables are normalized by the standard conditions; pressure = 2116.2 lbf/ft^2, temperature = 519 ^{o}R, and the speed of sound = 1116.8 ft/s.

Unsteady flow solution

Using the steady background flow described in the previous section and the gust harmonic content given in benchmark problem, LINFLUX was executed to calculate the harmonics of the unsteady response produced as a result of the impingement of the gust on the cascade. For each harmonic component of the gust (i.e., *n* = 1 to 3), the code was run until the residual level had reached the round-off error region. This required almost 20,000 iterations for the first harmonic, little over 33,000 iterations for the second harmonic, and nearly 12,000 iterations for the third harmonic. In every case, the size of the residual was reduced by at least six orders of magnitude.

Samples from the unsteady response are shown in Figure 3, 4 and 5. As before, the $x - \theta$ plane corresponding to the radial grid index = 4 is unrolled and duplicated. This time, however, the harmonic solution (for each *n*) is shifted by $\exp(ijn\sigma)$ for the jth passage, where $\sigma = 2\pi B/V$ is the so-called inter-blade phase angle and *i* is the square root of -1. The quantity *B*/*V* denotes the relationship between the gust and cascade periods in the *y*-direction which, using

the information supplied in the benchmark problem can be readily shown to equal 22/54 over a 2π period. It is convenient to interpret *B* and *V* as the blade and vane counts for the annulus problem. Then, in view of the Tyler-Sofrin rule, $m = nB - kV$ (where *k* is an integer), the modal structure of the response can be interpreted. The computed unsteady field includes both acoustic and convective modes. The acoustic modes, which correspond to $k = 0$, $k = 1$ or both, propagate at the speed of sound relative to the medium in both directions. The convective modes always correspond to $k = 0$ and travel at the speed of the background flow (i.e., are convected by it). The pressure field is comprised of acoustic modes only, while the velocity field includes both acoustic and convective modes, but tends to be dominated by the latter. The dominant acoustic modes produced in response to each gust frequency are listed in Table 2. The computed response is evanescent (i.e., cut-off) at the primary frequency, a deliberate design feature of the benchmark problem. The conversion from the 3D mode orders to the 2D wavenumbers is through the relation $k_y^{(a)} = m / \bar{R}$ where the superscript (*a*) denotes the acoustic wavenumber.

Frequency	Annulus Mode Order (3D)	Mode Wavenumber (2D)	Mode Type
ω	$m = +22$	$\hat{k}_y^{(a)} = +3.84$	Evanescent
	$m = -32$	$\hat{k}_y^{(a)} = -5.59$	Evanescent
	$m = +22$	$\hat{k}_y^{(c)} = +3.84$	Convected
2ω	$m = -10$	$\hat{k}_y^{(a)} = -1.75$	Propagating
	$m = +44$	$\hat{k}_y^{(c)} = +7.68$	Convected
3ω	$m = +12$	$\hat{k}_y^{(a)} = +2.09$	Propagating
	$m = -42$	$\hat{k}_y^{(a)} = -7.33$	Propagating
	$m = +66$	$\hat{k}_y^{(c)} = +11.52$	Convected

Table 2. The dominant unsteady response modes in the annulus and their two-dimensional transverse wavenumber equivalents. The 2D wavenumbers are normalized by the vane chord. The acoustic response at the primary frequency is cut-off. The convected mode wavenumbers (denoted by the superscript (*c*)) are multiples of the input gust wavenumber $11\pi/9$.

In Figure 3 the response to the incident gust corresponding to the primary frequency $\omega = 3\pi / 4$ is shown. The real part of pressure perturbation is shown on the left, and the real part of the axial component of velocity perturbation is shown on the right. The pressure and velocity perturbations are normalized by the inflow plane static pressure and steady velocity which can be obtained from Table 1. The pressure response, which is cut-off at this frequency, is dominated by two evanescent acoustic modes $m = +22$ and $m = -32$. The perturbation velocity field is dominated by the convected gust and thus is mainly comprised of $m = +22$ convected mode. The incident gust is distorted as it passes through the cascade. Note that the axial velocity perturbations are essentially out of phase downstream of the vane leading edge, and there is a jump in axial velocity across the wake sheet downstream of the trailing edge. It should be noted that the jump is not an artifact of the numerical dissipation discussed earlier, but a feature of the physical problem.

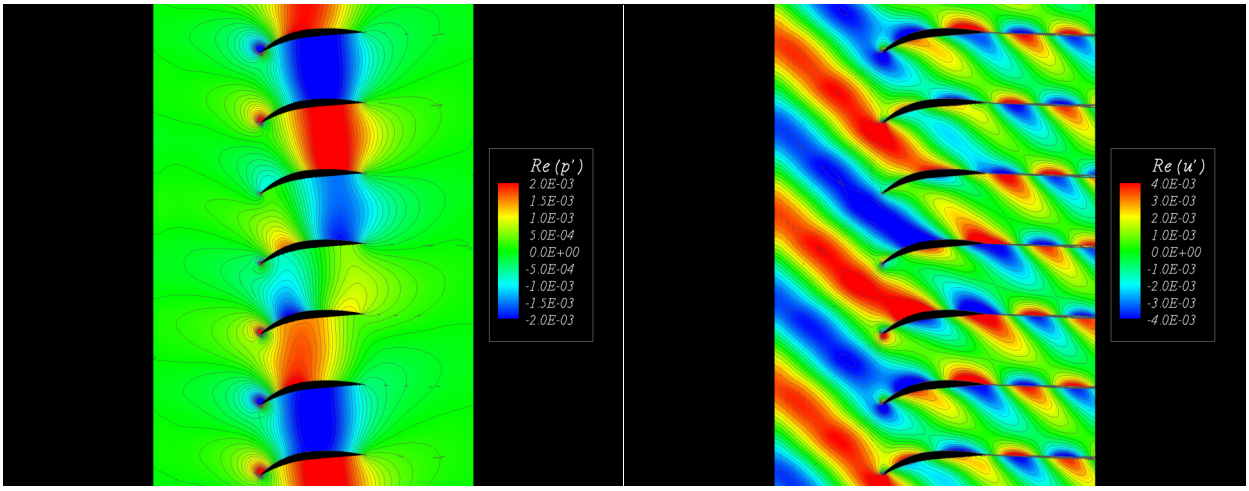

Figure 3. The computed response due to the gust at the primary frequency (i.e., $\omega = 3\pi/4$). Real part of the pressure perturbation is shown on the left and real part of the axial velocity perturbation is shown on the right. The pressure response is cut-off at this frequency and includes two evanescent acoustic modes $m = +22$ and $m = -32$. The perturbation axial velocity field is dominated by the convected gust and is mainly comprised of $m = +22$ convective mode.

Figure 4 shows the corresponding plots for the calculated response at twice the primary frequency. The pressure field at this frequency is due to a single propagating acoustic mode $m = -10$ with the wave fronts clearly evident away from the cascade especially at the exit plane. The axial velocity field is dominated by the convective mode $m = +44$ exhibiting twice as many wave fronts as that in Figure 1. Note the change in scale for both the pressure and velocity plots.

Finally, Figure 5 shows the calculated response at three times the primary frequency. The pressure field at this frequency is comprised of two propagating acoustic modes $m = +12$ and $m = -42$. The axial velocity field at this frequency is due to the convective mode $m = +66$ exhibiting three times as many wave fronts as that in Figure 1. Note the change in scale for both the pressure and velocity plots. The pressure wave fronts are not as clearly discernable as in Figure 4 due to interference between two contributing acoustic modes.

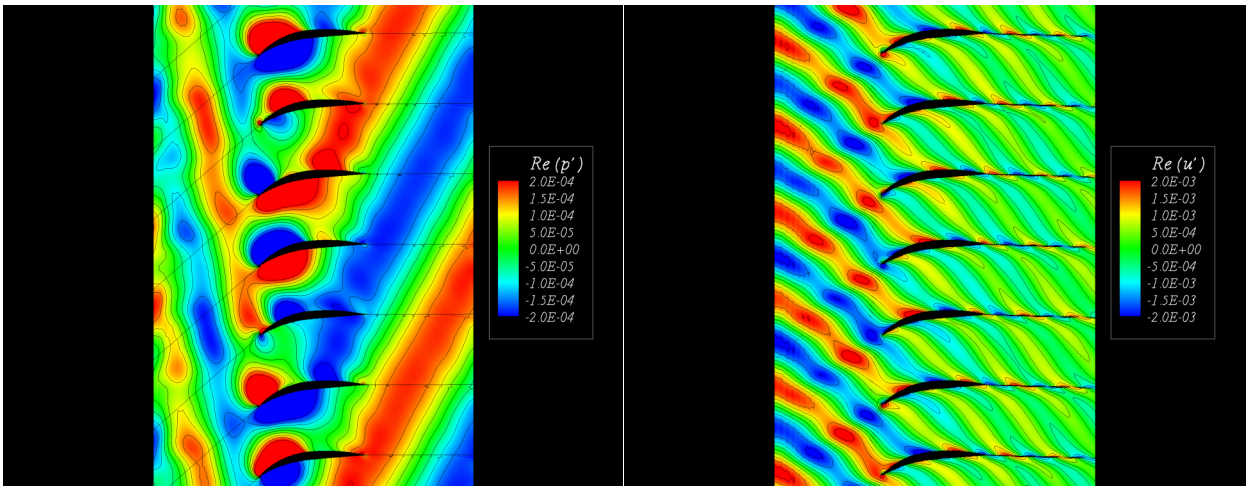

Figure 4. The computed response due to the gust at the twice the primary frequency. The pressure field is entirely comprised of the propagating (i.e., cut-on) acoustic mode $m = -10$. The axial velocity perturbation is due to the $m = +44$ convective mode.

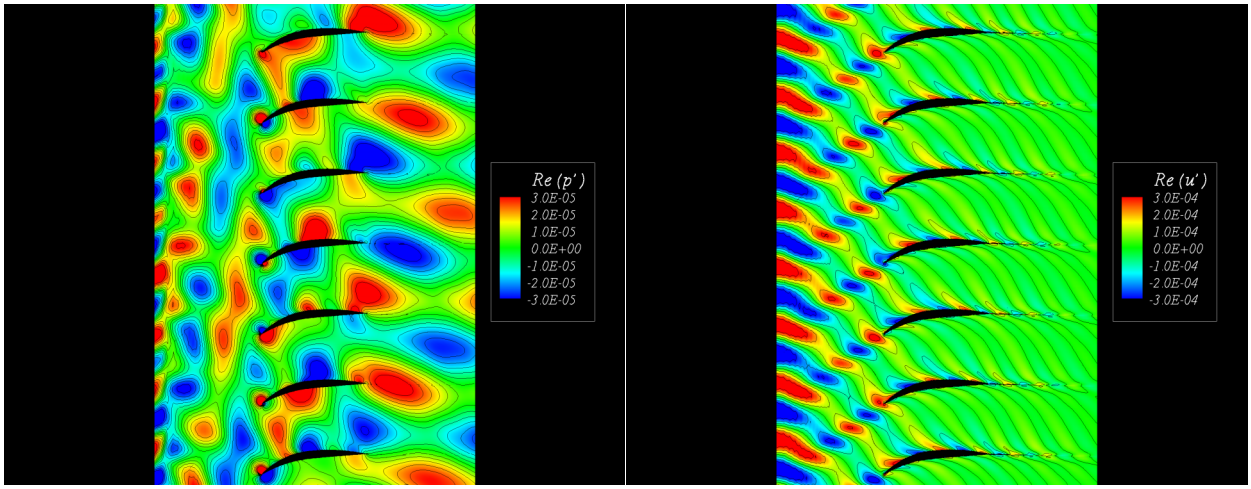

Figure 5. The computed response due to the gust at three times the primary frequency. The pressure response is comprised of two propagating acoustic modes m = +12 and m = -42. The axial velocity perturbation field is due to the m = +66 convective mode.

Computed spectra and mode information

In Tables 3 through 5 pressure levels for select locations in the domain are listed per requirements of the benchmark problem. All levels are expressed in dB using the standard definition of sound pressure level (SPL) given by 20 $\log_{10}(p_{rms} / p_{ref})$ where p_{ref} = 20 μPa. The complete solution package, including both steady and unsteady parts of the flow, is supplied on the workshop proceedings CD.

Frequency	Suction Side SPL (dB)			Pressure Side SPL (dB)		
	x/c = –0.25	x/c = 0.00	x/c = +0.25	x/c = –0.25	x/c = 0.00	x/c = +0.25
ω	140.7	140.6	141.2	138.0	141.5	140.5
2ω	128.3	118.4	121.0	128.6	121.4	119.5
3ω	104.1	107.5	92.8	104.5	103.0	97.6

Table 3. Acoustic pressure spectrum on the vane.

Frequency	Inflow Plane SPL (dB)			Outflow Plane SPL (dB)		
	y/c = –0.30	y/c = 0.00	y/c = +0.30	y/c = –0.30	y/c = 0.00	y/c = +0.30
ω	111.9	106.6	110.9	109.5	107.8	107.2
2ω	113.2	119.3	116.2	119.6	119.4	119.3
3ω	105.6	105.4	103.7	99.7	98.4	101.5

Table 4. Acoustic pressure spectrum at the inflow and outflow planes.

Frequency	Dominant Acoustic Pressure Modes	Inflow Plane SPL (dB)	Outflow Plane SPL (dB)
ω	$m = +22$	101.3	108.4
	$m = -32$	113.0	83.8
2ω	$m = -10$	116.8	119.2
3ω	$m = +12$	97.6	95.6
	$m = -42$	88.1	98.0

Table 5. Acoustic pressure modal amplitudes at the inflow and outflow planes.

REFERENCES

1. Montgomery, M.D. and Verdon, J.M.: A 3D Linearized Unsteady Euler Analysis for Turbomachinery Blade Rows, Part 1: Aerodynamic and Numerical Formulations; Part 2: Unsteady Aerodynamic Response Predictions. Published in Unsteady Aerodynamics and Aeroelasticity of Turbomachines, T.H. Fransson (ed.), pp. 427-464, Kluwer, Dordrecht, Netherlands, 1998.
2. Verdon, J.M.: Linearized Unsteady Aerodynamic Analysis of the Acoustic Response of Wake/Blade-Row Interaction. NASA/CR–2001-210713, 2001.
3. Prasad, D. and Verdon, J.M.: A Three-Dimensional Linearized Euler Analysis of Classical Wake/Stator Interactions: Validation and Unsteady Response Predictions. International Journal of Aeroacoustics, vol. 1 no. 2, 2002.
4. Envia, E.: Application of a Linearized Euler Analysis to Fan Noise Prediction. Presented at Fan-Gust Workshop, Institute of Sound and Vibration Research, University of Southampton, U.K., 2002. (http://www.isvr.soton.ac.uk/FDAG/fangust/)
5. Janus, J.M.; Horstman, H.Z.; and Whitfield, D.L.: Unsteady Flowfield Simulations of Ducted Propfan Configurations. AIAA Paper 92-0521, 1992.